June 8, 2000

CONCEPTUAL DESIGN OF THE SNS ENGINEERING DIFFRACTOMETER

X.-L. Wang
Spallation Neutron Source, Building 7964H, MS 6430
Oak Ridge National Laboratory, Oak Ridge, TN 37831-6430
wangxl@ornl.gov

SNS Report No. IS-1.1.8.2-6035-RE-A-00

1. EXECUTIVE SUMMARY

At the recommendation of the SNS Instrument Oversight Committee, conceptual design work has been undertaken for an engineering materials diffractometer as a potential candidate for inclusion in the initial suite of instruments. Scientific cases for this instrument were established by the user community at a number of workshops and have been summarized in a report by Holden et al.[1] A search has been initiated for a resounding and philosophical name for this instrument. At the moment, the instrument is tentatively named VULCAN, after the Roman god of fire and metalworking. Although the primary use of VULCAN is intended for deformation and residual stress related studies, other uses include spatial mapping of chemistry, microstructure, and texture.

The desired performance for VULCAN as determined by the user community are listed below.

- rapid volumetric (3-dimensional) mapping with a sampling volume of 1 mm^3 and a measurement time of minutes
- very high spatial resolution (0.1 mm) in one direction with a measurement time of minutes
- ~20 well defined reflection for in-situ loading studies
- ability to study kinetic behaviors in sub seconds
- simultaneous characterization capabilities, including dilatometry, weight, and microstructure
- ancillary equipment such as furnace and load frame be an integrated part of the instrument

Together, these requirements call for a "compound" engineering diffractometer with a large degree of flexibility for intensity-resolution optimization. The design philosophy is therefore to deliver a diffractometer with the highest desirable Q-resolution over a large angular range. For experiments that do not require such a high resolution, the incident beam divergence can be relaxed for intensity gain at the sample position. The key to this design is an interchangeable guide-collimator system.

The baseline design is schematically shown in Fig. 1a. This is a 44-m long instrument, consisting of a 3 m in-monolith guide, a frame definition chopper, a 20 m curved guide followed by a 12 m straight guide, and a 5 m interchangeable guide-collimator system. All guides are m3 supermirror guides and have a cross-section of 12×50 mm^2. The interchangeable guide-collimator system consists of five 1 m segments, each containing two channels which is either a m3 supermirror guide or a straight collimator. Each channel can be translated into the beam position at the push of a button. These channels are used in combinations to produce an incident beam of desirable divergence. A 1 m space is allowed between the sample and the exit of the guide-collimator system. In addition to housing the incident slit unit, this space may also be used to accommodate additional shielding or collimators. The detectors cover 60°-150° in 2θ and ±30° in the vertical plane. They are located on a locus designed to give an approximately equal resolution across the covered 2θ range. The radius of the detector locus ranges from 1.5 m at 150° to 5 m at 60°. Fig. 1b shows a three-dimension view of the instrument in the target building.

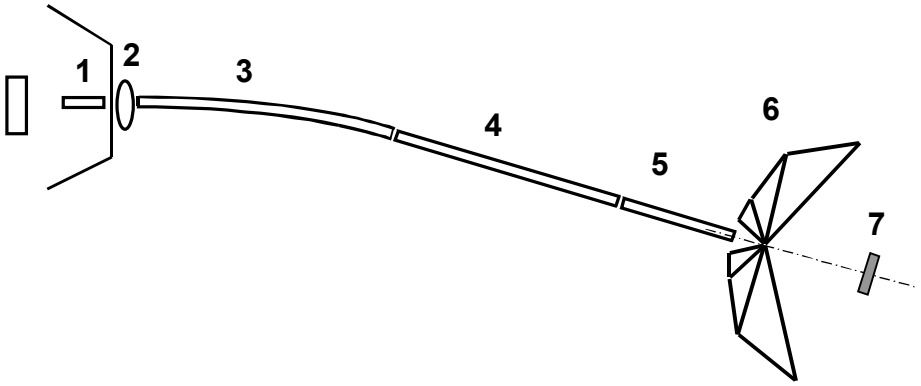

Fig. 1a Schematic of the base line design for VULCAN. The basic components and their characteristics are given below.
1 - in-monolith guide (supermirror, 3 m)
2 - frame definition chopper
3 - m3 curved guide (20 m)
4 - m3 straight guide (12 m)
5 - interchangeable unit (5 m)
6 - detector banks (variable distance to sample, 60°-150º in 2θ, ±30° in vertical plane)
7 - SANS detector (4 m from sample, 1 mm resolution)

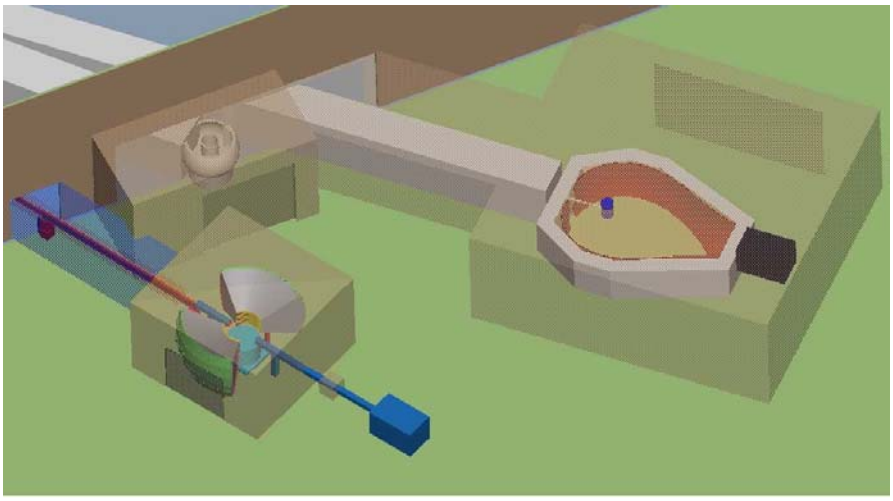

Fig. 1b A three-dimension view of VULCAN in the target building.

VULCAN can be operated flexibly for experiments having very different intensity-resolution requirements. In the high intensity mode, the m3 supermirror channel will be employed in all segments of the guide-collimator system, effectively extending the supermirror guide all the way to 1 m from the sample. This is the preferred mode of operation for most stress mapping experiments where the specimens already exhibit

significant peak broadening due to deformation, for kinetic studies where time resolution is critical, and for texture studies where a high Q-resolution is unnecessary. Note that even in this mode, the resolution is still quite good, ranging from 0.2% for 2θ=150º to 0.65% for 2θ=60º at *d*=1 Å. For comparison, the resolution for ENGIN, currently the only dedicated engineering diffractometer at a pulsed neutron source, is 0.7%. For in-situ loading studies where one needs to examine the response of individual reflections, however, it may be necessary to operate the diffractometer in the high resolution mode. In this mode, the collimator channel will be employed in all segments of the guide-collimator system, which produces a resolution of 0.10-0.22% *for all detectors*. This resolution is already better than that of the 148° (highest resolution) detector bank on GPPD at IPNS, which is sufficient to resolve ~ 20 peaks for cubic materials, such as Fe and Al, and for low-symmetry materials, such as Al_2O_3. Table I summarizes the performance matrix for these two vastly different operation modes. If the spatial variation is not of interest, as is the case for most in-situ loading experiments, the loss of neutron intensity can be more than compensated with the use of a large sample. For a 60 Hz target, the wavelength bandwidth is Δλ~1.3 Å, which can be positioned anywhere in the incident beam spectrum. If necessary, this bandwidth can be doubled by eliminating every other pulse using the frame definition chopper, effectively operating the instrument at 30 Hz.

Table I. Performance matrix for selected instrument configurations for a peak at *d*=1 Å.

	d=1 Å	High Intensity Mode (*)		High Resolution Mode	
Detector 2θ (º)	λ (A)	Relative Flux (%)	Δd/d (%)	Relative Flux (%)	Δd/d (%)
60	1.000	100	0.55	31	0.21
90	1.414	100	0.38	27	0.20
120	1.778	100	0.27	25	0.18
150	1.932	100	0.18	23	0.15
SANS Q range		0.01-0.18 $Å^{-1}$			
(*) Base line reference for intensity comparison.					

A 20×20 mm^2 two-dimensional position sensitive detector will be mounted at 4 m downstream for simultaneous diffraction and small angle measurements. By using a small specimen (e.g., < 5 mm width), a poor-man's SANS can be realized with little disruption to the base-line design. The Q-range was estimated to be 0.01 $Å^{-1}$-0.18 $Å^{-1}$. When desirable, a larger Q-range can be obtained by eliminating every other pulse using the frame definition chopper. A separate detector can be mounted at the center of the SANS detector to record

the transmission data. By analyzing Bragg edges in the transmission data, it is possible to obtain information about the chemistry and lattice strains in materials within the incident beam path. While methods for systematic analysis of the transmission data have not been fully developed, this technique has the potential for making measurements an order of magnitude faster than with the conventional diffraction method.

A great challenge lies in developing the technology that enables diffraction measurements with a 0.1 mm spatial resolution. Radial collimators, currently the method of choice at pulsed neutron sources for defining the sampling volume, becomes inefficient when used to define a 0.1 mm wide diffracted beam. This is because in today's technology, the minimum blade thickness is 0.1 mm. As part of the research efforts, two technologies will be pursued in parallel to achieve the 0.1 mm spatial resolution, one based on reducing the blade thickness of radial collimator and the other based on a novel Bragg mirror imaging concept.

2. DESGIN CONSIDERATIONS

2.1 Survey of similar instruments

VULCAN is the first and currently the only such planned "compound" diffractometer that is specifically designed to tackle a broad range of problems in engineering materials science with different intensity-resolution requirements. Nevertheless, a number of specialized instruments, e.g., high precision stress diffractometers *or* high intensity texture diffrctometers, are available for this survey:

Both reactors and pulsed neutrons have diffractometers for study of stress in engineering materials. A typical stress diffractometer at a reactor uses a monochromatic beam whose band width is given by

$$\frac{\Delta\lambda}{\lambda} = \cot\theta_m \cdot \Delta\theta_m , \qquad (1)$$

where $2\theta_m$ is the scattering angle of the incident neutron beam from the monochromator. On the scattering space (λ-2θ) diagram as shown in Fig. 2, this is represented by a horizontal band across 2θ. If the acceptable incident divergence is 1º, as is typically the case, then for a 90º monochromator take-off angle, $\Delta\lambda/\lambda \approx 1\%$. For NRSF at the HFIR, λ=1.5–1.6 Å and $\Delta\lambda \leq 0.02$ Å. On a pulsed neutron source, the incident spectrum has a broad wavelength band *but so far only detectors close to 90º were used for data collection.* In Fig. 2, this is represented by a vertical box centered at 2θ=90º. The ENGIN diffractometer at ISIS has a 2θ range of ±6º. Its upgrade, ENGIN-x, will have twice the angular coverage. The SMARTS diffractometer at LANSCE, currently under construction, has ±10º detector coverage in the scattering plane and ±20º in the vertical plane. Neutron guides are used in both instruments to transport neutrons over large incident flight paths (30 m for SMARTS and 50 m for ENGIN-x).

For texture determination, it is now generally accepted that pulsed neutron sources are far more efficient than reactor sources, despite the fact that time-averaged neutron flux at reactors is usually much higher. A state-of-the-art instrument for texture determination is represented by the HIPPO diffractometer at LANSCE. HIPPO features a short (9 m) incident beam flight path and a large detector array of about 1,400 ^{3}He detector tubes covering nearly a 4.6 m^2 area with five detector banks distributed at scattering angles ranging from back-scattering (nominally 150°) to forward scattering (nominally 10°). The detector panels are tilted relative to the diffracted neutron paths to give a more constant resolution across their surfaces. This tilt compensates for the change in resolution caused by the angular placement of each panel with a corresponding change in the sample-to-detector flight path. The 90° detector bank covers more than 3/4 of the Debye-Scherrer cone. It is estimated that with HIPPO, a complete pole figure can be determined with only a few rotations of the sample in less than 10 minutes.

For kinetic studies that requires medium resolution, the state-of-the-art instrument is perhaps the GEM diffractometer at ISIS. GEM has an incident flight path of 17 m. The special features of GEM include a large detector area (~10 m^2), which covers scattering

angles from 5° to 170°, and high degree of collimation of both incident and scattered beams. GEM has been designed to be a high-flux powder diffractometer with good resolution ($\Delta d/d$=2-3×10^{-3} for back scattering and $\Delta d/d$=5×10^{-3} at 90º). The data collection speed for GEM was demonstrated with a 8 mm YAG: a refinable data set was obtained in seconds.

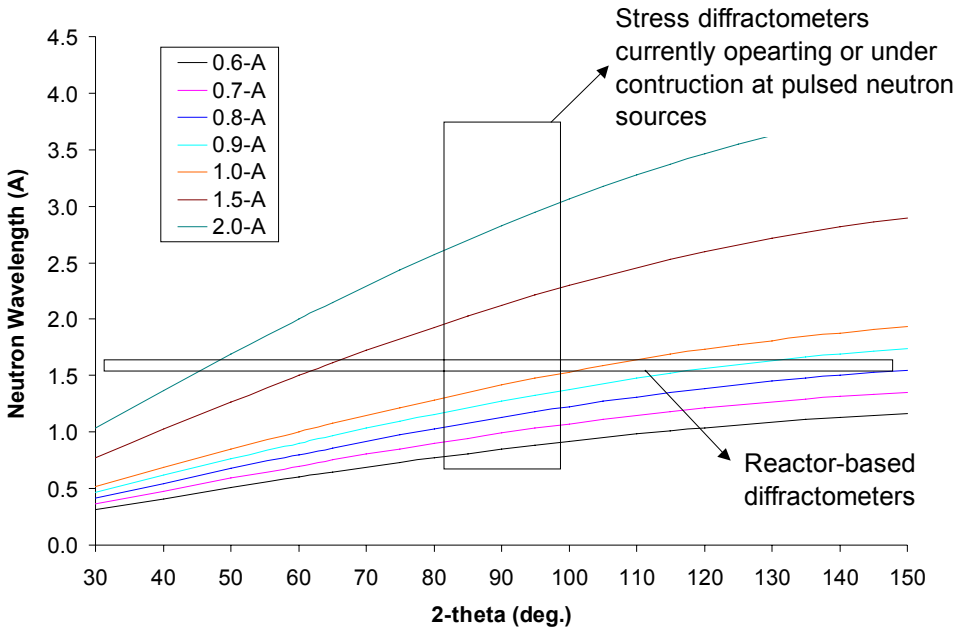

Fig. 2 Scattering space diagram illustrating the design philosophy for stress diffractometers that are currently operating or under construction at other neutron sources. The lines are Bragg's law calculated for various d-spacings.

No survey was done for small angle diffractometers. The SANS' attachment for VULCAN was configured using a spreadsheet program by Dr. J. K. Zhao, who is leading the design of the SANS instrument at SNS.

An optimized time-of-flight engineering diffractometer should utilize the scattering space to the fullest extent so long as the collected data are usable. From the above survey, it is clear that large detector coverage is used to its advantage in instruments designed for medium- or low-resolution kinetic and texture experiments. However, only limited detector coverage near 90º scattering angle is used in existing instruments designed for the measurements of stress. To derive an optimized design for VULCAN, it is essential to analyze the extent to which off-90º detectors can be used effectively in measuring stress. Specific questions include,

(1) How large is the error in the measured strain introduced by an uncertainty in defining the scattering vector?
(2) For a detector at 2θ≠90º, what is the difference between the scattering volume (or sampling volume) seen by this detector and that seen by the 90º detector?

These questions are addressed in sections 2.2 and 2.3 below.

2.2 Effect of averaging over strain components

In a neutron diffraction experiment, the strain value determined by a particular detector is the normal strain component along the scattering vector. When more than one detector is used, the experimentally determined strain value is an average of all strain components measured by individual detectors. To calculate the error introduced by this averaging, consider first the two-dimensional case where a detector bank spans over $2\theta \pm \phi$. The corresponding scattering vector spans over $\pm\phi/2$, as shown in Fig. 3. The strain value measured by this detector bank is an average given by

$$\langle \varepsilon_{33} \rangle = \frac{\int \varepsilon'_{33}(\phi')d\phi'}{\int d\phi'} \tag{2}$$

where,

$$\varepsilon'_{33} = \varepsilon_{33}\cos^2\phi' + \varepsilon_{13}\sin 2\phi' + \varepsilon_{11}\sin^2\phi'. \tag{3}$$

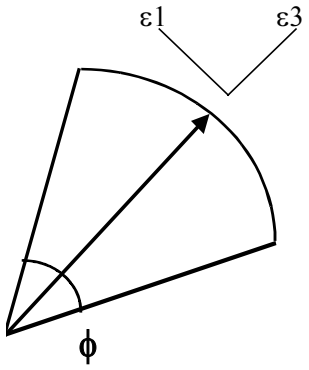

Fig. 3 Schematic diagram showing the effect of averaging over scattering vectors.

Carrying out the integration, one obtains

$$\langle \varepsilon_{33} \rangle = \frac{1}{2}\left(1 + \frac{\sin\phi}{\phi}\right)\varepsilon_{33} + \frac{1}{2}\left(1 - \frac{\sin\phi}{\phi}\right)\varepsilon_{11} \approx \varepsilon_{33} + \frac{\phi^2}{12}(\varepsilon_{11} - \varepsilon_{33}). \tag{4a}$$

Thus the error introduced by the use of a detector bank with an angular span ϕ is given by

$$\Delta\varepsilon_{33} \approx \frac{\phi^2}{12}(\varepsilon_{11} - \varepsilon_{33}). \tag{4b}$$

If out-of-plane detectors are also considered, then

$$\Delta\varepsilon_{33} \approx \frac{\phi^2}{12}(\varepsilon_{11} - \varepsilon_{33}) + \frac{\psi^2}{12}(\varepsilon_{22} - \varepsilon_{33}), \tag{5}$$

where ψ is the angular range of out-of-plane detectors. This error is largest when ε_{33} and ε_{11}, ε_{22} have opposite signs. To quantify this effect, consider the worst case scenario: an uni-axial loading of high strength steel whose yield strength can be as high as 800 MPa. The

loading direction is assumed to be along axis-3 in Fig. 3. The Young's modulus and Poisson's ratio for steel is approximately E = 200 GPa and ν=0.3. Hooke's law gives ε_{33}=4000 and $\varepsilon_{11}=\varepsilon_{22}$=-1200 microstrains. Suppose six measurements were made to determine the full strain tensor along the principal axes and in directions bisecting the principal axes. It can be shown that the errors in the experimentally determined strain tensor are

$$\begin{pmatrix} -13 & -13 & 7 \\ & -13 & 7 \\ & & 26 \end{pmatrix}, \qquad \text{when } \phi=\psi=10°$$

$$\begin{pmatrix} -30 & -30 & 15 \\ & -30 & 15 \\ & & 59 \end{pmatrix}, \qquad \text{when } \phi=\psi=15°$$

$$\begin{pmatrix} -53 & -53 & 26 \\ & -53 & 26 \\ & & 106 \end{pmatrix}, \qquad \text{when } \phi=\psi=20°$$

Keeping in mind that the precision in a strain measurement is typically 100 microstrains, it is safe to conclude that detectors distributed within a 15° or less apex cone can be grouped together to increase the data rate for the measurement of strains. Alternately, one may chose to combine the detectors in smaller groups and use them separately. In this case, strain data obtained from separate detector groups will facilitate the determination of the stress tensor.

2.3 Change in scattering volume at off-90° diffraction angles

When a detector is positioned at an off-90° angle, the scattering volume becomes a parallelepiped. As shown in Fig. 4, this volume is different from that seen by the 90° detector. The latter is a square. It can be shown that at a given scattering angle 2θ, the total amount of dissimilar areas, highlighted in Fig. 4 by the hatches, reaches a minimum value when $x_1=x_2$. Under this condition, the scattering volume S is given by

$$S = \frac{1}{2} W^2 \cot(2\theta) \tag{6}$$

At 2θ=60º, S/W^2=29%. This means that a detector at 2θ =60º sees about 70% of the scattering volume that a 90º detector sees. Note that in this optimal configuration, $W' \neq W$. In stead, W' is related to W by,

$$W' = W \sin(2\theta). \tag{7}$$

For 2θ=60º, W'=0.87W. In conclusion, from scattering volume point of view, detectors as low as 60º or as high as 120º can be used together with 90º detectors in stress mapping experiments.

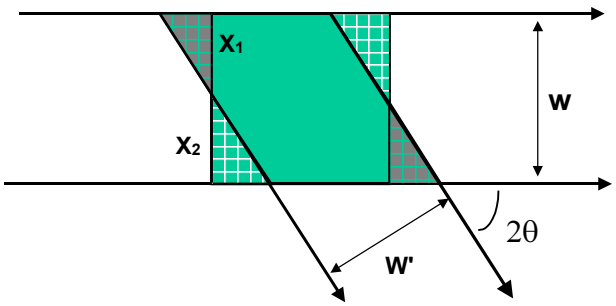

Fig. 4 Schematic illustrating the change in scattering or sampling volume for detectors at $2\theta \neq 90°$.

2.4 Figure of merit

Because of the differences in the desired performance for different types of experiments, VULCAN needs to be optimized for multiple figure of merit. For texture and kinetic studies, the instrument should be optimized for intensity. Meanwhile, this instrument must also have, or at minimum can provide, sufficient resolution to separate ~20 peaks for in-situ loading studies. Examination of diffraction data collected at GPPD at IPNS and ENGIN at ISIS indicates that for common engineering materials, such as Fe, Al, Al_2O_3, a resolution of $\Delta d/d = 2\text{-}3\times10^{-3}$ will suffice.

In strain measurements, one is primarily interested in the relative change in the peak position, δd/d. An analysis based on the Bayesian approach (details provided in Appendix A) shows that the figure of merit for the determination of δd/d is given by

$$FM = \frac{\lambda^4 \Phi(\lambda)}{4\sin\theta \cdot R^2} \cdot \cot\theta \cdot \Delta\theta \cdot Z \cdot F^2(\tau) \cdot f \cdot \frac{SN}{SN + \sqrt{8}} \quad . \qquad (8)$$

The various symbols in Eq. (8) are described below.

$\Phi(\lambda)$	incident neutron spectrum
$\Delta\theta$	angular spread by the detectors
Z	multiplicity of the peak
$F(\tau)$	unit-cell structure factor
f	fraction of the Debye-Scherrer cone covered by the detectors
R	resolution function (see section 2.5)
SN	signal to noise ratio

The term $\frac{SN}{SN + \sqrt{8}}$ is a discount factor due to the presence of a slow-varying background. Numerical results for the discount factor are shown in Fig. 5. It can be seen that the discount factor increases as SN improves, leading to a greater overall figure of merit.

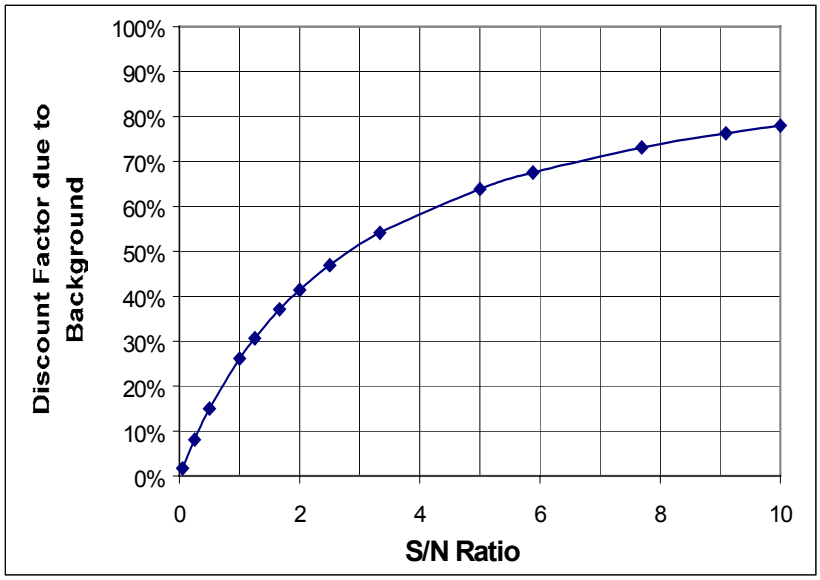

Fig. 5 Discount factor for the figure of merit due to the presence of a slow-varying background.

Eq. (8) shows clearly which quantities should be optimized for an instrument designed for strain measurement. For an idealized instrument,

(1) the incident spectrum should exhibit maximum flux for the set of diffraction peaks of interest;
(2) the resolution function should be minimized for the same set of diffraction peaks;
(3) the background should be suppressed to minimum.

Conclusions (1) and (2) provide guidance for the choice of moderators, which is discussed in further detail in section 3.1. Together, conclusions (2) and (3) suggest a very long incident flight path since both resolution (see section below for detailed discussions) and background improves with an increase in the total flight path. When neutron guide is used, the loss in neutron flux can be quite small. Thus there will be an increase in the figure of merit. However, one factor that has not been considered in Eq. (8) is the coverage in d-spacing, which diminishes as the total flight path increases. For most engineering materials, the diffraction peaks of interest have a d-spacing of 0.5-2 Å. As shown in Fig. 6, to measure them with detectors at 2θ=60°-150° requires neutrons with a wavelength of 0.9-2.1 Å. Therefore, to ensure an adequate coverage in d-spacing, the total flight path for VULCAN should not exceed 50 m.

2.5 Resolution function

A simple analytical function is used to calculate the resolution for VULCAN. In this approach, the resolution, defined as $R = \frac{\Delta d}{d}$ where Δd is the FWHM of the peak profile, is calculated using the following equation,

$$\left(\frac{\Delta d}{d}\right)^2 = \left(\frac{\Delta t}{t}\right)^2 + \left(\frac{\Delta L_{total}}{L_{total}}\right)^2 + \left[\left(\frac{W_{\det}}{L_{scatt}}\right)^2 + \left(\frac{W_{sample}}{L_{scatt}}\right)^2 + \Delta\theta_{inc}\right]\cdot\cot^2\theta\,, \qquad (9)$$

where Δt/t is the moderator pulse width divided by the total neutron flight time, and the various W's and L's are the widths and path lengths indicated (all converted to FWHM where appropriate). $\Delta\theta_{inc}$ is the divergence of the incident beam at the sample position. Despite its simplicity, Eq. (9) reproduces rather well the measurement results obtained for GPPD at IPNS and the Monte Carlo simulation results for SMARTS at LANSCE. Eq. (9) suggests that to achieve high resolution, one should have

- small pulse width
- long flight path
- small detectors
- small sample size
- large secondary flight path (from sample to detector)
- neutron guide terminated far from the sample

Additionally, an optimized design should have matching contributions from time and geometry.

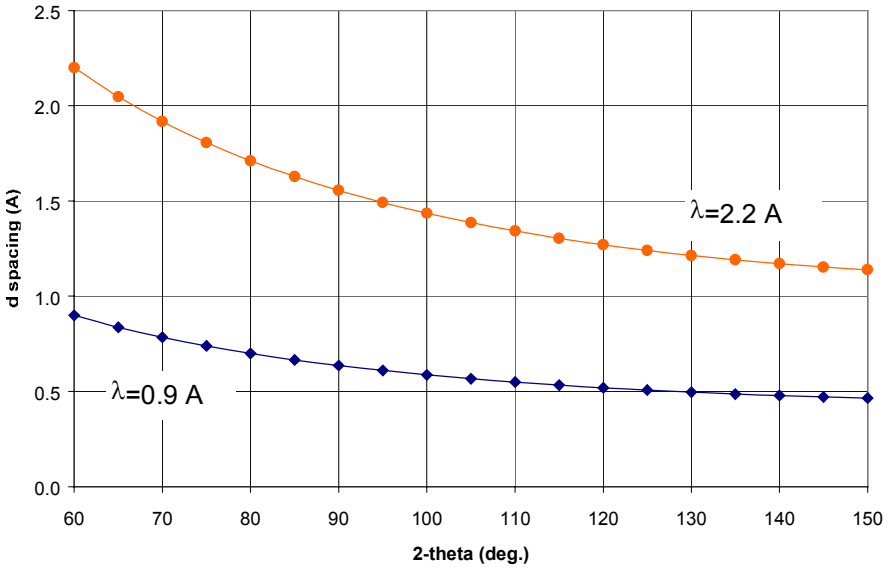

Fig. 6 d-spacing coverage for incident neutrons with wavelengths from 0.9 to 2.2 Å.

2.6 Achieving 0.1 mm spatial resolution

Achieving the 0.1 mm spatial resolution is a great challenge. Radial collimators, currently the method of choice at pulsed neutron sources for defining the sampling volume, become inefficient when used to define a 0.1 mm wide diffracted beam. This is because in today's technology with stretched Mylar, the minimum blade thickness is 0.1 mm. However,

with the advances in optical coatings technology, it may be possible to reduce the overall blade thickness by depositing neutron absorbing materials onto a thin substrate or onto Si.

Alternate imaging techniques will also be pursued. One that shows great promise is a novel concept called Bragg mirror imaging proposed by A. D. Stoica. A Bragg mirror is made of elastically bent silicon crystals. Depending on crystal cutting angles, thickness, and bending curvature, a sample can be imaged in real space with a position sensitive detector. A particular feature of this device is that the spatial resolution is determined to a large extent by the thickness of the Si plates. With Si wafers, which are commercially available, a 0.1 mm spatial resolution can be achieved. In addition, with the crystal used as an analyzer, the signal to noise ratio is significantly improved, which is essential for the measurements of diffraction from a small sampling volume.

Earlier tests done at HFIR using monochromatic neutron beams have demonstrated the feasibility of imaging with 1 mm spatial resolution. Research is currently underway to further develop this technique. An unresolved question is the operating wavelength bandwidth, i.e., whether the device bandwidth is large enough to take advantage of a broad energy spectrum provided by a pulsed neutron source. Although analytical calculation indicates that the operating wavelength bandwidth can be as high as 10%, this must be demonstrated experimentally. Also, position-sensitive detectors with a 0.1 mm resolution, which presently do not exist, must also be developed.

The forgoing considerations have led to a baseline concept for VULCAN, which will be discussed in more detail below. A key component in this conceptual design is an interchangeable guide-collimator system. Table II lists the basic components and pertinent parameters for VULCAN.

Table II. Basic components and the pertinent parameters for VULCAN

Component	Type & Properties	Starting distance from moderator (m)
Moderator	Ambient temperature water, de-coupled and poisoned	0
In-monolith guide	m3 supermirror Straight Length – 3m Guide width – 12 mm Guide height – 50 mm	2
Frame definition chopper	Disk chopper Operating frequency: variable 10-60 Hz Radius to beam center – 250 mm Beam width at chopper – 12 mm	5
Curved guide	m3 supermirror Curved (20 straight sections) Length – 20m Guide width – 12 mm Guide height – 50 mm Radius of curvature – 2 km	6
Straight guide	m3 supermirror Straight Length – 12m Guide width – 12 mm Guide height – 50 mm	26
Interchangeable Guide-collimator system (*) current design, which will evolve as other options are examined.	Interchangeable unit Total length – 5 m Number of segments – 5 Number of channels per segment – 2 (*) Channel width – 12 mm Channel height – 50 mm Channel length – 1 m Coatings on channel #1 Top and bottom – m3 supermirror Sides – m3 supermirror No coatings on channel #2	38

Component	Type & Properties	Starting distance from moderator (m)
Shielding/Collimator	Length – 1 m	43
Aperture	Various sizes Retractable along incident beam path	43-44
Sample	Width – 0.1 to 10 mm (but must be < 5 mm for simultaneous diffraction and SANS measurements)	44
Detectors	60°-150° continuous coverage in scattering plane ±30° in the vertical plane Width – 6 mm for 60° to 80° detectors 12 mm for all other detectors Distance to sample – variable, e.g., 60° – 5 m 90° – 4 m 120° – 2.3 m 150° – 1.5 m	
SANS detector	2D position sensitive Dimension – 20×20 mm^2 Resolution – 1 mm	48
Bragg edge detector	> 100 MHz count rate	48

3. PRELIMINARY ASSESSMENT OF PERFORMANCE

3.1 Moderator

At present, the ambient temperature water moderator (poisoned and de-coupled) was selected for VULCAN because of its sharp pulses and high flux in the desirable wavelength range, i.e., λ~1 Å. However, this choice may change as other types of moderators become available. Fig. 7 shows the MCNP simulation results for the selected moderator.

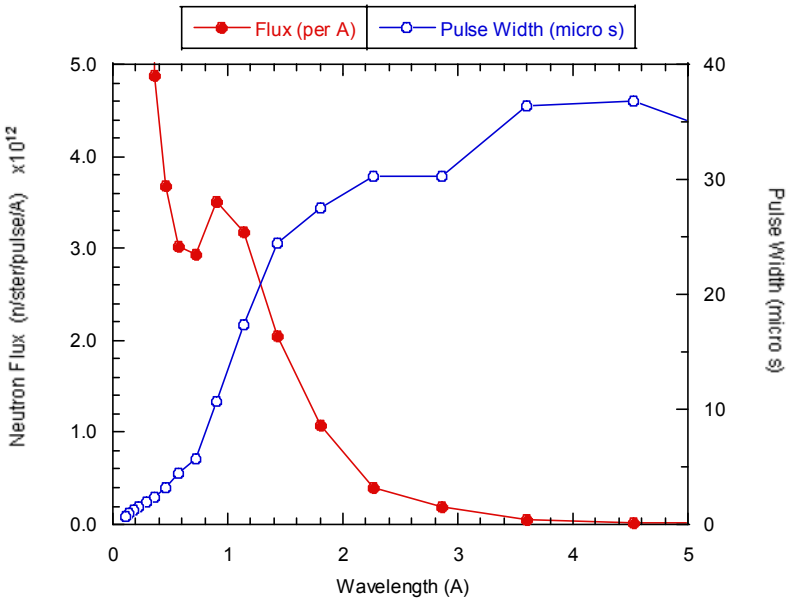

Fig. 7 MCNP simulation results for the ambient temperature water moderator (poisoned and de-coupled).

3.2 Chopper

A chopper with adjustable opening and variable operating frequency will be used to define the wavelength bandwidth for VULCAN. To minimize the leak of unwanted neutrons, this chopper should be installed as close to the moderator as possible, i.e., just outside the biological shielding. Different wavelength band is defined by rephasing the chopper with the source. Fig. 8 shows a representative chopper timing diagram for defining a λ=0.9-2.2 Å bandwidth. The first instance of 'leak' in this operation occurs at λ~15 Å, where the neutron flux is 10^7 times weaker.

3.3 Neutron guides

A long curved guide is used to suppress the transmission of high energy (E>eV) neutrons at the sample position. Calculations shows that for a 20 m guide with a curvature radius of 2 km, the moderator will be well out of line of sight. In general, high critical angle coating is required in order to improve the transmission of neutrons at short wavelength (e.g., 1 Å).

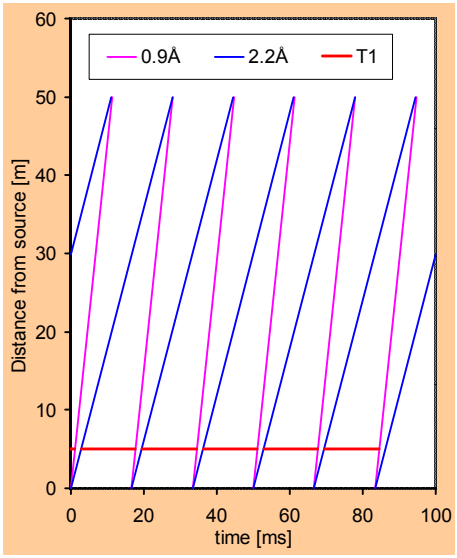

Fig. 8 Chopper timing diagram illustrating the definition of a λ=0.9-2.2 Å bandwidth.

Fig. 6 shows Monte Carlo simulation results illustrating the effect of curvature on neutron transmission. As can be seen, high energy neutrons (E>eV) are greatly suppressed. The transmission efficiency increases to more than 80% for 1-Å neutrons and almost 100% at 3 Å and above. It is anticipated that with the use of a curved guide, a T_0 chopper will not be necessary.

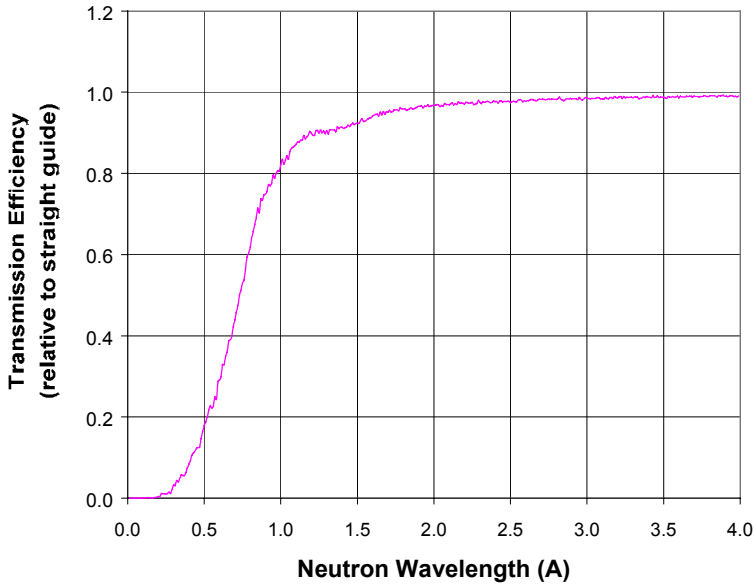

Fig. 6 Ratio of the number of neutrons transmitted through a curved guide versus the number of neutrons through a straight guide

A straight m3 supermirror guide is used to 'scramble' the anomalous angular distribution of neutrons emerging from a curved guide. Monte Carlo simulation shows that after 5 m of straight guide, the angular distribution became more or less symmetric again. In the current design, the straight guide section is 12 m.

3.4 Interchangeable guide-collimator system

A detailed design for the guide-collimator system has not been decided. Presently, the system is made of five 1-m segments, each having two channels separated by shielding materials. One of the channels is coated with m3 supermirror on the sides, while the other has no coating. The top and bottom of both channels are coated with m3 supermirror. Each channel can be translated into beam position at the push of a button, and channels in different segments are used in combinations to produce an incident beam of desirable divergence. Monte Carlo simulation was used to assess the influence of various operation configurations on intensity and resolution. The results are illustrated in Figs. 9-10 for three configurations: (1) 5m guide, or high intensity mode, (2) 5 m collimation, or high resolution mode, (3) 3 m guide followed by 2 m collimation. These are labeled as 0, 2, and 5 m collimation, respectively. As can be seen Fig. 9, the high resolution mode is accompanied with a factor of 2-5 loss in intensity. Fig. 10 shows the horizontal divergence (FWHM) of the incident neutron beam at the sample position. With 5 m collimation, the FWHM of the incident beam is 0.11°. Natural collimation, with a FWHM~0.06°, is reached when the guide is terminated at 10 m from the sample. Monte Carlo simulation for this configuration shows a further decrease in neutron intensity, by a factor of two.

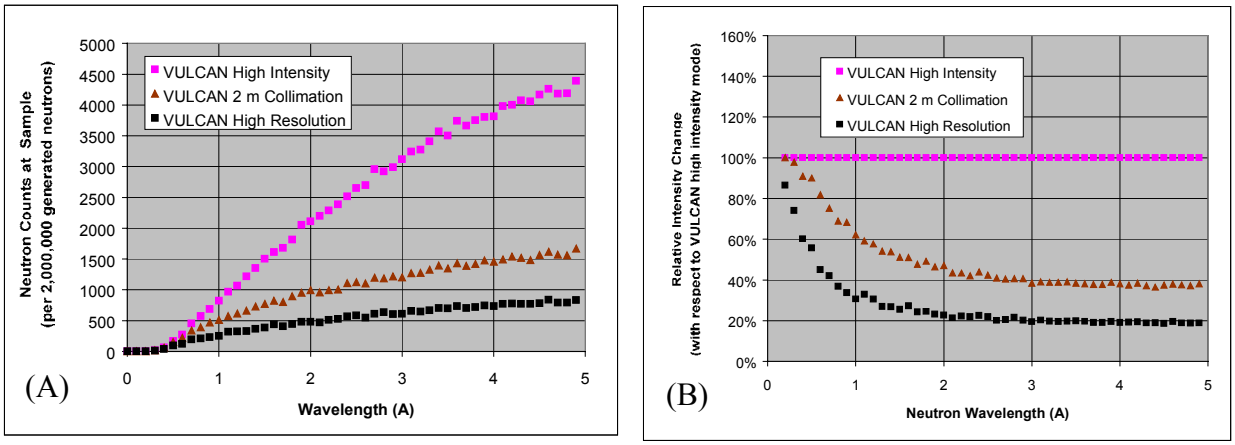

Fig. 9 Monte Carlo simulation to assess the performance of the guide-collimator system for selected operating configurations. (A) Neutron counts at sample. (B) Relative intensity change with VULCAN high intensity mode as the baseline. The neutron source is a Lambert source with a uniform flux as a function of neutron wavelength. A 5×30 mm^2 sample is assumed. The frame definition chopper was not considered in this simulation.

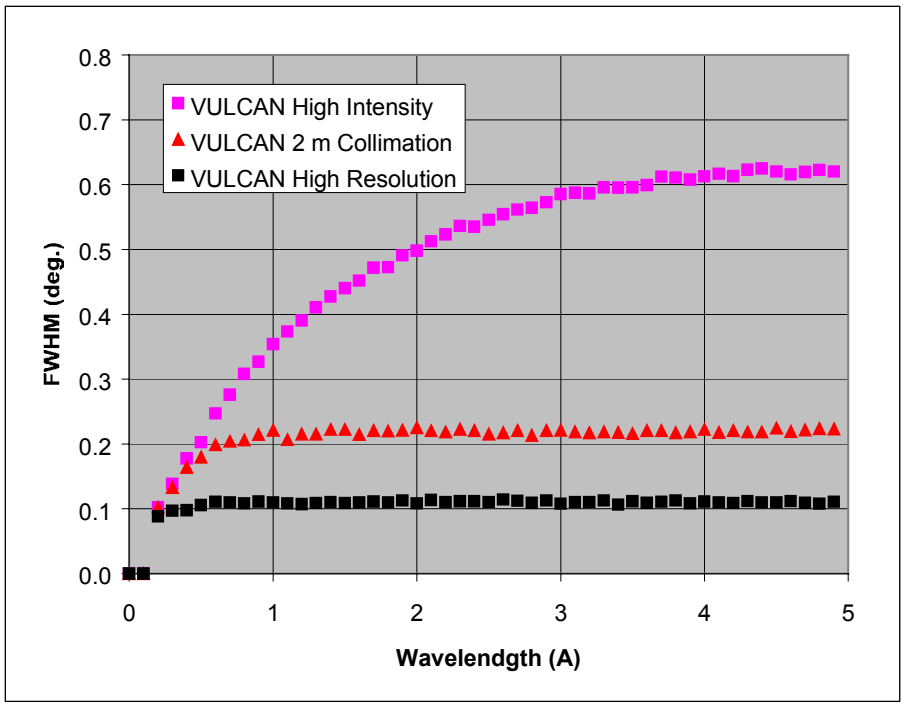

Fig. 10 Monte Carlo simulation results for the FWHM of the incident neutron beam in the horizontal scattering plane for selected operating configurations of the guide-collimator system.

3.5 Resolution

The resolution function for VULCAN is calculated using Eq. (19), again for three configurations discussed earlier and is shown in Fig. 11. The resolution in the high resolution mode (Fig. 11(C)) varies from 0.1% to 0.22% in the range of d-spacings of interest to engineering materials. In this mode, the contributions from time and geometry are matched for all four detectors under study (2θ=60°, 90°, 120°, 150°). The resolution improves only slightly if the guide is terminated at 10 m from the sample. In the case of the 90° detector, for example, the resolution changes from 0.20% to 0.18% at d=1 Å. For comparison, the resolution function for the 148° detector bank of GPPD is also shown. As indicated earlier, the resolution of GPPD is already sufficient to resolve ~ 20 peaks for most engineering materials.

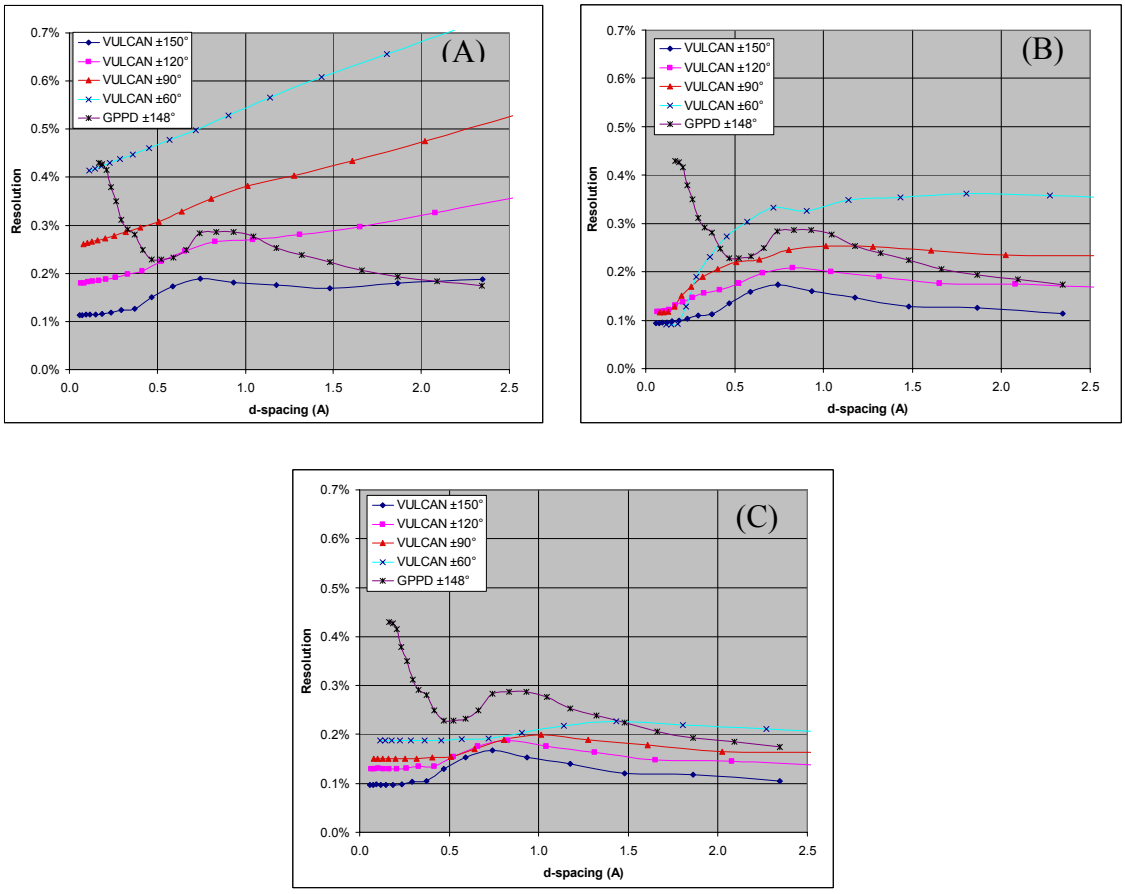

Fig. 11 Resolution function ($R = \frac{\Delta d}{d}$, where Δd is the FWHM of the peak profile) for VULCAN at various 2θ values: (A) high intensity mode; (B) 2 m collimation; (C) high resolution mode. For comparison, the resolution function for the 148° detector bank of GPPD is also shown. The GPPD resolution is sufficient to resolve ~ 20 peaks for most engineering materials. The top scale of 0.7% is the resolution of ENGIN at ISIS.

4. PERFORMANCE COMPARISON

A performance comparison has been made with two state-of-the-art instruments: NRSF at HFIR and SMARTS which is under construction at LANSCE. As discussed earlier, the gain over reactor instruments is mainly through the use of a larger wavelength bandwidth. For VULCAN, with detectors ranging from 60° to 150°, a peak at d=1 Å is measured with a bandwidth of $\Delta\lambda$~0.93 Å. For NRSF, this bandwidth is approximately 0.02 Å and the peak is measured with detectors on the focusing side only. Thus, with the same source, the gain for VULCAN would be 2×0.93/0.02 = 93. However the time-averaged flux at HFIR is five times that at SNS. In addition, a novel focusing technique in the horizontal scattering plane helps NRSF to gain another factor of two in neutron flux. Considering these factors, the real gain for VULCAN over NRSF is ~10, for a single peak at d=1 Å. This gain will be

multiplied by a factor of 10-20, the number of reflections accessible to VULCAN detectors. Thus, the overall gain over NRSF is in the rang of 100.

To compare with SMARTS, a Monte Carlo simulation was performed using the design parameters as of August 1999, which are listed in Table III. To assess the performance of the neutron guide system, the SAME neutron source and sample was used. As in the simulation for VULCAN, the two choppers in SMARTS were ignored. The simulated neutron intensity per 2,000,000 generated neutrons is plotted in Fig. 12, along with the results for VULCAN. The horizontal FWHM is plotted in Fig. 13. It can be seen that with the same source, VULCAN and SMARTS have similar neutron intensity. At VULCAN's primary operating wavelength range of 0.9-3.0 Å, VULCAN shows a gain up to 60% due to the use of m3 supermirror coating on the sides. SMARTS has a slightly higher intensity at longer wavelength (λ>3 Å). It is interesting to note that the FWHM for SMARTS varies linearly with λ, This is probably due to the use of a wider guide and a short guide-to-sample distance. The resolution function is compared in Fig. 14 for the 90° detectors (SMARTS is designed with one detector bank centered at 90°).

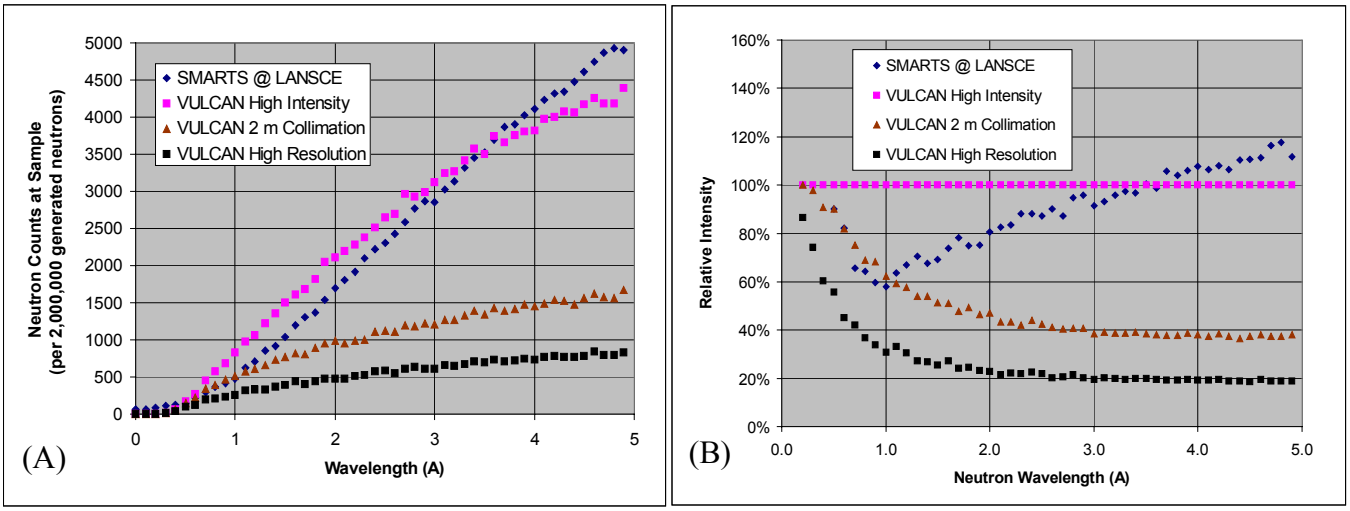

Fig. 12 Monte Carlo simulation to compare the performance of the neutron guide system between SMARTS and VULCAN. (A) Neutron counts at sample. (B) Relative intensity with VULCAN high intensity mode as the baseline. The neutron source is a Lambert source with a uniform flux as a function of neutron wavelength. A 5×30 mm^2 sample is assumed. Choppers were not considered in either simulations.

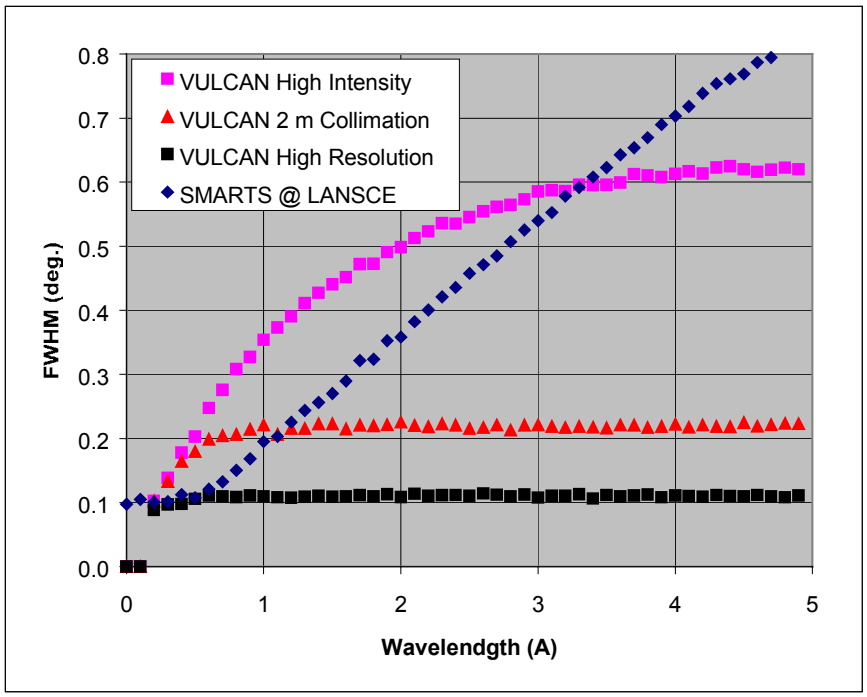

Fig. 13 Monte Carlo simulation results to compare the FWHM of the incident neutron beam in the horizontal scattering plane between SMARTS and VULCAN.

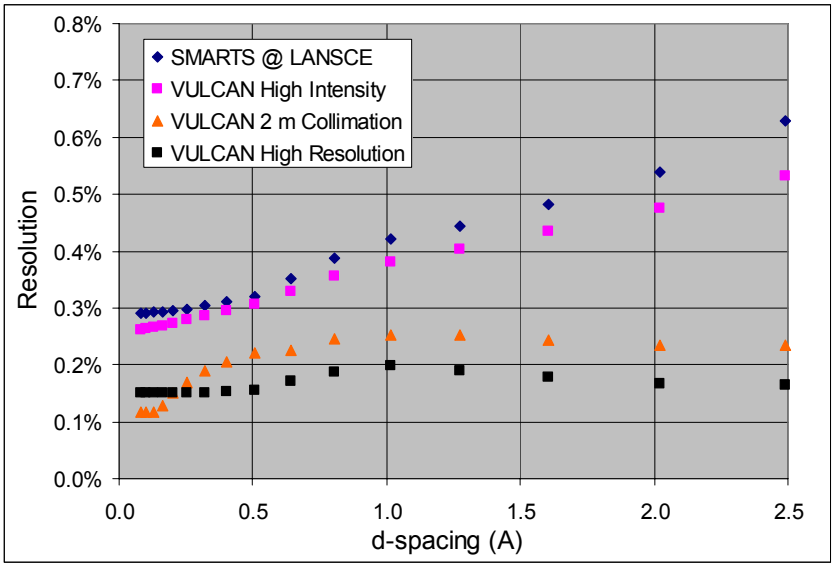

Fig. 14 Comparison of the resolution function between SMARTS and VULCAN for the 90° detectors.

Table III. Instrument parameters for SMARTS (as of August 1999) used in Monte Carlo simulations for comparison with VULCAN

Component	Type & Properties	Starting distance from moderator (m)
Moderator	Ambient temperature water, de-coupled and poisoned (?)	0
In-monolith beam pipe	Absorbing wall Straight Length – 4 m Guide radius – 60 mm	1
T_0 chopper	Length – 0.3 m	5
Straight guide	Natural Ni (m1) on the sides m3 supermirror at the top and bottom Length – 4.7 m Guide width – 50 mm Guide height – 50 mm	5.3
Frame definition chopper	Disk chopper Operating frequency: variable 10-60 Hz Length – 0.3 m Radius to beam center – 500 mm Beam width at chopper – 50 mm	10
Straight guide	Natural Ni (m1) on the sides m3 supermirror at the top and bottom Length – 18.7 m Guide width – 50 mm Guide height – 50 mm	10.3
Exit aperture	0.5 m from the end of the neutron guide Width 10 mm Height 50 mm	29.5
Sample	0.5 m from the exit aperture Radius 5 mm Height 10 mm	30
Detector	80-100° continuous coverage in 2θ ±20° in the vertical plane Distance to sample – 1.5 m	

A calculation is also made to compare the figure of merit (Eq. (8)) for the 90° detectors at various d-spacing. The results are summarized in Table IV. It is seen that VULCAN shows a universal gain of about 1.4-3 in the figure of merit over SMARTS. For strain measurements, this gain should be further multiplied by the ratio of useful detector coverage area, which gives another factor of 2-3, depending on the type of measurements. Taking into account the 10 times more intense source at SNS, a reasonable estimate of the overall gain over SMARTS will be in the range of 30-50.

Note that the among the three operation modes considered for VULCAN, the highest figure of merit is obtained when the instrument operates in the high resolution mode. The overall figure of merit decreases slightly when the instrument operates in the moderate resolution mode (with 2 m collimation). It should be kept in mind that these calculations are made for an ideal sample. When the sample exhibit an appreciable peak broadening, the figure of merit will decrease. For example, if the specimen exhibits a peak broadening of 0.5% in $\Delta d/d$, as is frequently observed in weld specimens, the figure of merit for the high resolution mode decreases by a factor 6-10. In this case, the high intensity mode should be used.

Another state-of-the-art instrument is ENGIN-x at ISIS. A computer model has not been set up for ENGIN-x so that a comparison could not be made at this time. However, one feature in the ENGIN-x design is the early termination of its m3 supermirror guide at 10 m from the sample to achieve best resolution. A simulation for VULCAN suggests that terminating the guide at 10 m from sample results in a factor of 2 loss in intensity whereas the resolution only improves marginally, by abut 10% for the 90° detector at d=1 Å.

Based on the comparisons with NRSF and SMARTS, achievable counting times for VULCAN have been estimated and listed in Table V.

5. ANCILLARY EQUIPMENT

A number of ancillary equipment has been requested by the user community to be an integrated part of the instrument. A partial list of basic equipment is given below.

- A versatile, heavy duty specimen manipulation table, including a three-dimensional translation stage, a rotary table, and a Euler cradle or Kappa unit
- Coordination machine for the determination of specimen geometry, especially for specimens of complex shape
- Load-frame with a furnace attachment for in-situ loading and fatigue studies
- Vacuum furnace up to 2000°C
- Laser alignment facility
- Collision avoidance system
- Laser dilatometer for simultaneous, in-situ characterization of dimensional change

Table IV. A comparison of SMARTS and VULCAN for selected instrument configurations. The comparison is made for the 90° detector only. The intensity comparison is based on Monte Carlo simulation results for the neutron guide systems. The SAME neutron source and sample were used in these simulations.

		SMARTS @ LANSCE			VULCAN High Intensity			VULCAN 2 m Collimation			VULCAN High Resolution		
d(Å)	λ (Å)	R	INT	FM	R	INT(*)	FM	R	INT	FM	R	INT	FM
0.51	0.72	0.32%	65%	63488	0.31%	100%	105895	0.22%	75%	154716	0.15%	42%	176071
1.01	1.43	0.42%	68%	38154	0.38%	100%	68575	0.25%	54%	84005	0.20%	27%	67987
2.02	2.86	0.54%	96%	33030	0.47%	100%	44410	0.23%	41%	73766	0.17%	20%	73736
2.49	3.52	0.63%	101%	25417	0.53%	100%	35398	0.23%	38%	70686	0.16%	20%	74190

(*) Baseline intensity.

Table V. Estimated counting times for different types of experiments proposed for VULCAN.

Experiment Type	Desirable Parameters	Achievable Counting Time
3D mapping	1 mm^3	2 minutes
1D mapping	0.1 mm	60 min. (*)
In-situ Loading	~20 well separated peaks	1 min
Kinetic Measurements		0.1 sec
Diffraction & SANS	0.01-0.18 $Å^{-1}$	sec
Bragg Edge (Transmission)		< 1 sec
(*) With the Bragg mirror technique, the entire depth profile is determined in one measurement.		

Most, if not all, of the equipment mentioned above should be reproduced in labs outside the target building for mounting, testing, and preliminary characterization of the specimens and special devices to be used in the neutron experiments. At minimum, there should be a mock-up unit of the specimen manipulation table so that a user can determine all necessary measurement coordinates and geometry prior to the neutron experiment. Users will also be encouraged to develop any special equipment (i.e., a quench furnace) for their particular experiments.

It is noted that most of the requested ancillary equipment is commercially available. For example, both MTS and INSTRON make excellent load-frames for tensile and fatigue tests. Furnace attachments with a temperature range up to 1500°C are also available and can be essentially "clipped" onto the unit. As another example, *in-situ* non-contact dilatation measurements, which are ideal for monitoring changes in sample's dimension due to, for example, phase transformation, can be carried out using laser interferometry-based dilatometer. In addition to the non-contact nature, this method also avoids the effect of a small elastic load that is applied to fix the "push rod" type dilatometer on the sample. In all cases, however, expert opinions will be sought to specify a unit suitable for use with VULCAN.

6. CHALLENGES AND R&D EFFORTS

Research efforts should proceed immediately on how to achieve the 0.1 mm spatial resolution for a class of important experiments proposed for VULCAN. Two technologies will be pursued in parallel to achieve this goal, one is based on improving the efficiency of

radial collimators and the other on the Bragg mirror concept. Much research is still needed to prove the feasibility of the Bragg mirror concept. But once proven, the technique will be fully implemented because it offers a tremendous advantage over the conventional methods in that an entire depth profile can be determined simultaneously

Other questions remain on the optimization of individual components and the entire instrument. These include:

1. what is the optimum guide width?
2. what is the effect of vertical focusing on intensity and resolution?
3. how to describe the resolution function of out-of-plane detectors?
4. how to to optimize the SANS attachment?
5. exactly what are the sampling volumes at different angles?
6. how to analyze Bragg edges and make use of the transmission data?

Setting up a full-scale Monte Carlo simulation program is a key to address many of these questoins.

7. REFERENCE

[1] T. M. Holden, http://www.sns.anl.gov/ScatInst/Instrument/EnDi.htm
[2] D. S. Sivia, "Data Analysis, a Bayesian Tutorial," Clarendon Press, Oxford University Press Inc., New York, USA (1996).

8. ACKNOWLEDGEMENT

I wish to thank everyone who attended the workshop on “Performance Requirements for the SNS Engineering Diffractometer,” held on January 20-21, 2000 at the Institute for Paper Science and Technology, Atlanta, Georgia. Excellent presentations were made by Dr. S. A. David and S. S. Babu, Professor D. McDowell, Dr. M. A. M. Bourke, Dr. Z. Feng, Dr. T. M. Holden, Professor E. Ustundag, Dr. C. H. Hsueh, Dr. M. R. Daymond, Professor B. Scholtes, Professor D. R. Clarke, Dr. C. R. Hubbard, Dr. J. W. Richardson, Professor P. J. Withers, Dr. I. C. Noyan, and Dr. B. Radhakrishnan. Most of the performance requirements described in this report were based on these presentations and ensuing discussions at the workshop. The Monte Carlo simulation work was carried out using IDEAS (which stands for Instrument Design and Experiment Assessment Suite) developed at the Oak Ridge National Laboratory. Special thanks are due to Dr. W.-T. Lee who helped to set up the Monte Carlo simulations program and made available the modules on various types of neutron guides.

APPEDIX A FIGURE OF MERIT FOR MEASUREMENT OF STRAIN

In strain measurements, one is primarily interested in the relative change in the peak position, δd/d. For a symmetric peak profile, the peak position is equal to the mean. Applying standard statistics, the deviation of the measured mean peak position from the true value, is given by

$$(\delta x)^2 = \frac{1}{N}\sum (x_i - x)^2 , \tag{A.1}$$

where N is the total number of neutron counts, or integrated intensity. When N is very large, x can be replaced by the measured mean and Eq. (A.2) becomes,

$$(\delta x)^2 \approx \frac{1}{N}\sum \left(x_i - \bar{x}\right)^2 . \tag{A.2}$$

Note that $\sum \left(x_i - \bar{x}\right)^2$ is the second moment of the peak profile, whose squared root is proportional to the full width half maxima, w. Thus, one has

$$(\delta x)^2 \propto \frac{w^2}{N} = \frac{w^2}{I}, \tag{A.3}$$

where I is the integrated intensity. Therefore, in order to minimize δx, one must maximize the figure of merit

$$FM = \frac{I}{w^2} . \tag{A.4}$$

Eq. (A.4) is also valid for asymmetric peak profiles. However, the position of an asymmetric peak profile is not necessarily characterized by the mean. Since diffraction peak profiles on pulsed neutron sources are usually asymmetric, it is important to ascertain whether Eq. (A.4) remains to be a valid figure of merit for the determination of peak positions.

Sivia [2] showed that a more generalized solution for the figure of merit can be found using Bayesian analysis. In the Bayesian analysis, the influence of the background can also be included. Formal treatment using Bayesian analysis shows that,

$$FM = \frac{I}{w^2} \cdot \frac{SN}{SN + \sqrt{8}} \tag{A.5}$$

for a Gaussian distribution [2] and

$$FM = \frac{I}{w^2} \cdot \left(1 - \frac{1}{SN}\ln(1+SN)\right) \qquad \text{(A.6)}$$

for an exponential decay profile. In both equations, SN is the signal to noise ratio. It can be seen that except for a discount factor due to the presence of a slow-varying background, Eqs. (A.5-A.6) are otherwise identical to Eq. (A.4),. Fig. A.1 shows the numerical results for the discount factors as a function of SN. As expected, the discount factors decrease with SN, leading to smaller values for the figure of merit. Moreover, this decrease accelerates when SN becomes smaller. Thus, to minimize the penalty of the discount factor, the background should be suppressed to a minimum whenever feasible.

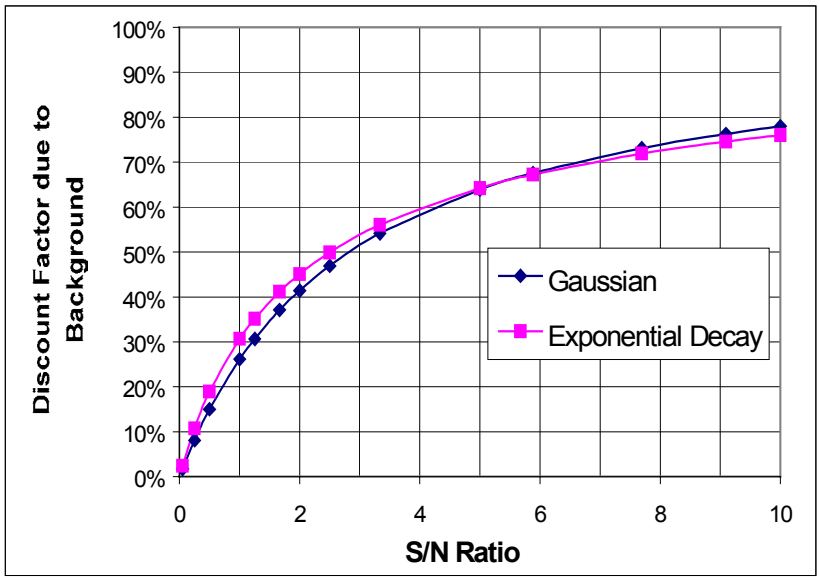

Fig. A.1 Discount factors for the figure of merit due to the presence of a slow-varying background. (See Eqs. (A.5-A.6) in text)

Although the discount factors in Eqs. (A.5-A.6) differ in analytical form, the numerical results are almost identical. In light of this similarity, Eq. (A.5) will be used throughout the this report for simplicity. In reality, the diffraction peak profiles on pulsed neutron sources is neither a Gaussian or an exponential decay profile, but to a first degree approximation can be modeled by a combination of both. Therefore it is reasonable to assume that their figure of merit is similar to Eqs. (A.5-A.6), which are now collectively written as,

$$FM = \frac{I \cdot d^2}{w^2} \cdot \frac{SN}{SN + \sqrt{8}} = \frac{I}{R^2} \frac{SN}{SN + \sqrt{8}}, \qquad \text{(A.7)}$$

where R=w/d is the resolution at a given d-spacing.

The integrated intensity for a diffraction peak is given by

$$I = \frac{\lambda^3 \Phi(\lambda)\Delta\lambda}{4\sin\theta} \cdot Z \cdot F^2(\tau) \cdot f \,, \qquad \text{(A.8)}$$

where F and Z are the unit-cell structure factor and the multiplicity of the Bragg reflection, respectively, f is the fraction of the Debye-Scherrer cone covered by the detectors, $\Phi(\lambda)$ is the incident neutron spectrum, and $\Delta\lambda$ is the wavelength band selected by the detector which is related to the angular spread of the detectors by

$$\frac{\Delta\lambda}{\lambda} = \cot\theta \cdot \Delta\theta \quad . \qquad \text{(A.9)}$$

Substituting Eq. (A.9) into (A.8), one obtains,

$$I = \frac{\lambda^4 \Phi(\lambda)}{4\sin\theta} \cdot \cot\theta \cdot \Delta\theta \cdot Z \cdot F^2(\tau) \cdot f \,. \qquad \text{(A.10)}$$

Substituting Eq. (A.9) into (A.7), an explicit expression for the figure of merit in strain measurements is obtained,

$$FM = \frac{\lambda^4 \Phi(\lambda)}{4\sin\theta \cdot R^2} \cdot \cot\theta \cdot \Delta\theta \cdot Z \cdot F^2(\tau) \cdot f \cdot \frac{SN}{SN + \sqrt{8}} \quad . \qquad \text{(A.11)}$$